nature geoscience

ARTICLES
https://doi.org/10.1038/s41561-021-00727-y

Check for updates

Long-lived shallow slow-slip events on the Sunda megathrust

Rishav Mallick[1,2] ✉, Aron J. Meltzner[1,2], Louisa L. H. Tsang[3,4], Eric O. Lindsey[2,5], Lujia Feng[2] and Emma M. Hill[1,2]

During most of the time between large earthquakes at tectonic plate boundaries, surface displacement time series are generally observed to be linear. This linear trend is interpreted as a result of steady stress accumulation at frictionally locked asperities on the fault interface. However, due to the short geodetic record, it is still unknown whether all interseismic periods show similar rates, and whether frictionally locked asperities remain stationary. Here we show that two consecutive interseismic periods at Simeulue Island, Indonesia experienced significantly different displacement rates, which cannot be explained by a sudden reorganization of locked and unlocked regions. Rather, these observations necessitate the occurrence of a 32-year slow-slip event on a shallow, frictionally stable area of the megathrust. We develop a self-consistent numerical model of such events driven by pore-fluid migration during the earthquake cycle. The resulting slow-slip events appear as abrupt velocity changes in geodetic time series. Due to their long-lived nature, we may be missing or mis-modelling these transient phenomena in a number of settings globally; we highlight one such ongoing example at Enggano Island, Indonesia. We provide a method for detecting these slow-slip events that will enable a substantial revision to the earthquake and tsunami hazard and risk for populations living close to these faults.

Tectonic slow-slip phenomena span a wide range of slip rates, from mm yr^{-1} to mm s^{-1}, and represent a mode of tectonic fault slip behaviour that can be detected by geodetic instruments but does not release the seismic radiation typically associated with earthquakes. While post-earthquake accelerated fault creep (afterslip), earthquakes deficient in high-frequency radiation (slow earthquakes) and spontaneous slow-slip events (SSEs) all fall under the purview of slow-slip phenomena, in this study we are concerned only with the kinematics and dynamics of SSEs. It is unclear whether SSEs are simply earthquakes in slow motion[1] or a separate group of phenomena caused by significantly different underlying mechanisms[2,3]. The most common hypothesis regarding the mechanics of SSEs on faults governed by frictional processes involves large earthquake (instability) nucleation sizes on velocity-weakening fault zones[4–8] in the presence of low effective confining stresses, which means that instabilities can nucleate but not run away to seismic slip rates. Such low confining stresses generally result from elevated pore pressures[3,9–11]. Additional SSE mechanisms include a switch from velocity-weakening behaviour at low velocities to velocity-strengthening behaviour at higher velocities[12,13], and the fluid-driven interplay of frictional and ductile processes at depths where rocks become hot enough that flow-like behaviour is activated[14–17].

Here we show that a decadal-scale SSE nucleated on a shallow velocity-strengthening section of the Sunda megathrust. Velocity-strengthening faults are generally thought to be stable, and therefore unable to nucleate frictional instabilities such as earthquakes and SSEs[18,19]. The observations and inferences we present challenge the typical model of SSE nucleation and therefore necessitate a different mechanism to explain its kinematics.

Transient deformation in the Simeulue coral record

In this study, we focus on the deformation history of Simeulue Island in the time period 1738–1861 (refs. [20,21]) (Fig. 1). This is thought to be an interseismic period for this section of the Sunda megathrust, leading up to a plate boundary rupture of M_w ~8.5 in 1861 (refs. [20,22]). The magnitude and spatial pattern of the coseismic deformation in the 1861 event bear remarkable similarity to the 2005 M_w 8.6 Nias–Simeulue megathrust earthquake[20,22], indicating that fault zone properties have remained largely static for at least two earthquake cycles. This implies that it is reasonable to use inferences of frictional properties from the better-documented earthquake cycle, the 2005 earthquake[23,24] (Fig. 1a), to study fault zone mechanics from the eighteenth to nineteenth centuries.

The shallow marine corals on Simeulue record the combined effects of long-term sea-level and land-height change. These corals recorded a linear subsidence at a rate of 1–2 mm yr^{-1} from 1738 to 1829 (Figs. 1b and 2a). Around 1829 (±3 years), an abrupt velocity change occurred at each of the coral sites (Extended Data Fig. 1), causing significantly greater subsidence rates of up to 10 mm yr^{-1} (Figs. 1b and 2a), which persisted until the great earthquake in 1861. Previous studies have shown that these velocity changes are tectonic in origin, and interpreted them as spontaneous variations in the spatial extent of frictionally locked asperities and stably creeping regions of the Sunda megathrust[20,21]. Specifically, the locked section of the megathrust was thought to have expanded down-dip to a depth of ~55 km (ref. [21]). While variations in dimensions of locked asperities have been interpreted to occur on megathrusts in relation to stress transfer from nearby earthquakes[25,26], there is no evidence to suggest that moderate/great earthquakes occurred within ~500 km of Simeulue around the time of the

[1]Asian School of the Environment, Nanyang Technological University, Singapore, Singapore. [2]Earth Observatory of Singapore, Nanyang Technological University, Singapore, Singapore. [3]Université Côte d'Azur, CNRS, Observatoire de la Côte d'Azur, IRD, Géoazur, Campus CNRS, Sophia Antipolis, Valbonne, France. [4]Present address: International Study Centre, University of Surrey, Guildford, UK. [5]Present address: Department of Earth and Planetary Sciences, University of New Mexico, Albuquerque, NM, USA. ✉e-mail: rishav001@e.ntu.edu.sg

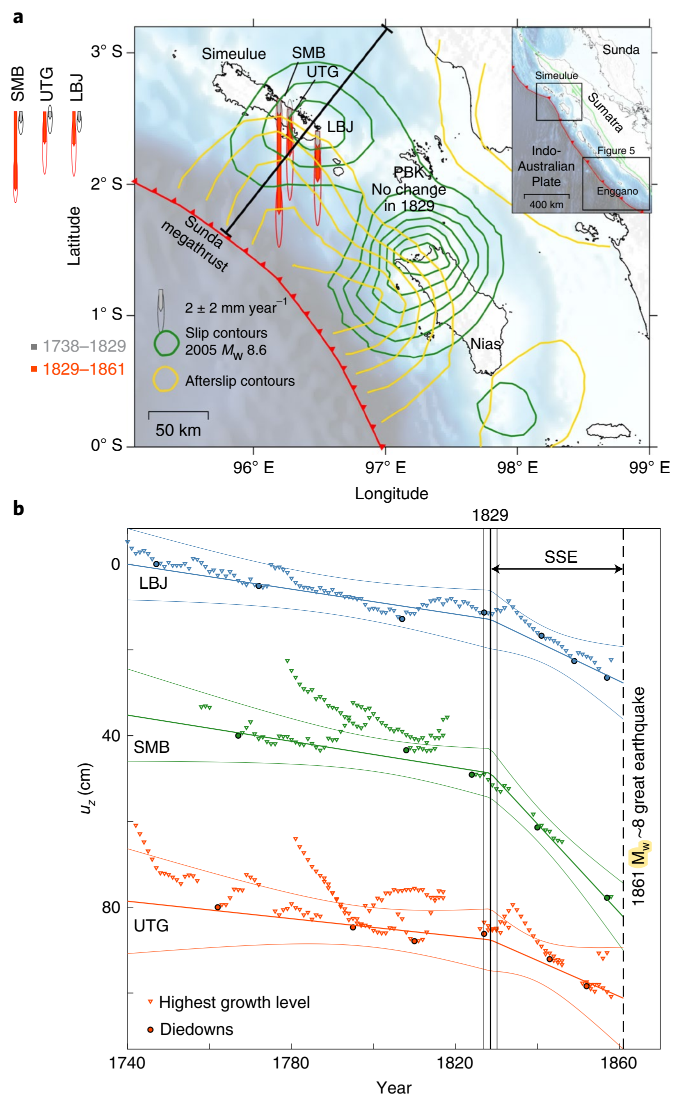

Fig. 1 | Tectonic setting of the study (inset map). a, The 2005 M_w 8.6 Nias–Simeulue earthquake ruptured a portion of the Sunda megathrust, as shown by the coseismic slip (green contours, 2 m intervals) and post-earthquake creep (yellow contours, 0.5 m intervals)[23]. The three coral sites we use in this study are labelled LBJ, SMB and UTG. We show computed velocities from 1738 to 1829 (grey) and 1829 to 1861 (red). The PBK site recorded no velocity change before or after 1829. The black line represents the cross-section we use in the 2D approximation in Fig. 2. **b**, Time series of the coral growth rate (u_z) at three sites (1738–1861), and the estimated timing of the velocity change (1829 ± 3). Only the filled circles (the highest level of growth prior to each diedown)[20] are considered in the velocity estimation. Model predictions are shown by the thick lines, and 95% confidence intervals by thin line envelopes.

abrupt velocity change in the coral records[20,22]. Additionally, frictional locking is not expected to persist beyond the brittle–plastic transition, which is thermally controlled in subduction zones, and is estimated to be around 30 km deep for this location[27–29]. In light of these inconsistencies, we reevaluate the observations and inferences from the palaeogeodetic record for Simeulue using a physics-based inverse method to relate fault slip rates to subsidence rates, and test the hypothesis that steady frictional locking/sliding on a megathrust can explain the observed vertical deformation history.

Steady and unsteady interseismic behaviour

We develop an inverse method in which we solve for the locked ($v=0$) and unlocked ($v>0$) distribution of fault segments during each time period separately, for steady frictional behaviour on a megathrust driven by the stresses arising from subducting an elastic slab into the mantle (in-plane strain; see Methods). In our formulation, fault slip rates in the unlocked segments are governed by the stressing rates afforded by the nearby locked segments[30,31]; that is, we seek a simply connected locked domain, and the surrounding region is treated as a crack driven at constant stress (Extended Data Fig. 2a). This is inherently different from typical over-parameterized interseismic coupling inversions which solve directly for slip rates and are forced to use slip rate regularization to stabilize the inverse problem. We pose the inverse problem in terms of the misfit between the observed coral subsidence rates and the predicted rates as a function of the geometric parameters that describe the locked and unlocked domains. This is a nonlinear problem for which we employ a Markov chain Monte Carlo sampling scheme (see Methods for details).

From the inferred fault segment locking/unlocking distributions, we show that, under the assumption of piece-wise steady-state interseismic processes, a down-dip migration of the interseismically locked zone is necessary to fit the 1829–1861 coral data (Extended Data Figs. 2c and 3). This feature has been noted by previous studies[20,21]. Additionally, the previously locked shallow megathrust needs to unlock and remain that way, in order to improve the fit to the 1829–1861 subsidence rates (Extended Data Fig. 2b). However, this configuration is physically implausible for three reasons:

(1) The transition from down-dip frictional locking to creep at the full plate subduction velocity would need to occur over infinitesimally narrow widths on the megathrust (Extended Data Fig. 2d) in order to fit the 1829–1861 vertical velocities. This would create nearly infinite stressing rates which cannot be supported by the elastic medium.

(2) If the down-dip extent of the megathrust were to relock and remain in that configuration from 1829 to 1861, this must have been completed within 6 years (uncertainties in the timing of the velocity change) (Fig. 1b). This implies sustained creep deceleration of at least ~10 mm yr^{-2} on the megathrust at depths of ~30–50 km, followed by approximately three decades of elastic strain accumulation within a domain which is at temperatures greater than 500 °C (Extended Data Fig. 2c)[27,29]. We are currently unaware of any mechanism that can cause such a process spontaneously on a plate boundary fault or shear zone under these conditions; rock deformation at these temperatures is dominated by either viscous or plastic creep, not stick-slip.

(3) Earthquake cycle simulations show that unlocking of previously locked fault segments, as we infer for the shallow megathrust from our piece-wise steady-state inverse models (Extended Data Fig. 2b), does not occur abruptly. Gradual unlocking of frictional asperities is seen in numerical models when creep from the fault segments surrounding the asperity erodes its boundaries[32]. However, this process leads to nonlinear displacement time series[32–34], which is again inconsistent with our observations.

To explain the abrupt change in vertical velocities in the observational record, our preferred model is one where the locking configuration from 1738 to 1829 persisted on the fault, while a multi-decadal SSE spontaneously nucleated and was sustained on the shallow megathrust from 1829 to 1861 (Fig. 2 and Extended Data Figs. 3 and 4). We model this SSE as uniform velocity fault creep over a simply connected domain (Methods). We infer the plausible range of transient fault slip rates to be 0.7–2.5 times the long-term trench-normal convergence rate and the SSE released 0.8–3.0 m of slip (Fig. 2d). If we assume that this deformation occurred uniformly over the width

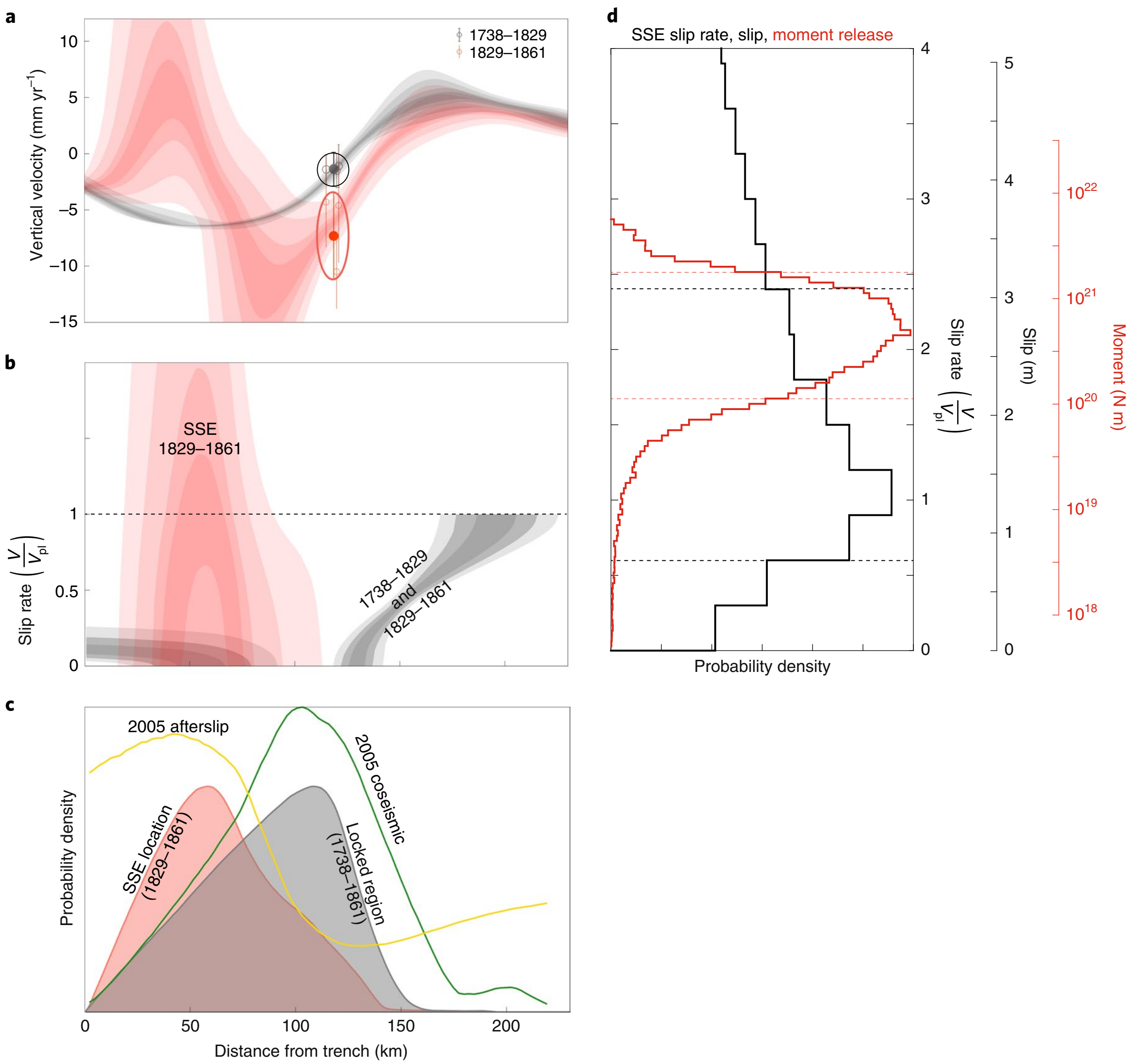

Fig. 2 | Observations and modelling results for the eighteenth- and nineteenth-century coral record at Simeulue projected along the cross-section shown in Fig. 1a. a, Subsidence rates for 1738–1829 (grey) and 1829–1861 (red), assuming that the velocities from each epoch collectively show the average response of southern Simeulue Island to tectonic changes (filled circles), with vertical velocities at individual sites (open circles with error bars) and model predictions (shaded bands for 67% confidence level, with darker colours showing envelopes closer to the median). **b**, Estimated slip rate (V/V_{pl}, where V_{pl} is the plate rate) for the two epochs considered. The data from 1738–1829 is modelled as a steady interseismic process (grey shaded bands). We model the slip rate for 1829–1861 as an SSE (red) superimposed on the existing slip rate distribution from 1738–1829. **c**, Comparison of the probability distribution of the locked region (grey) and SSE location (red) with qualitative estimates of velocity-weakening (green, coseismic) and velocity-strengthening (yellow, afterslip) regions inferred from the 2005 M_w 8.6 Nias earthquake[23], along the transect shown in Fig. 1a. **d**, Probability distributions of slip rate and slip of the shallow SSE (black) and the equivalent moment release (red) assuming a shear modulus of 30 GPa and along-strike width of 100 km.

of our transect (100 km), we predict a moment release equivalent to an event of M_w 7.2–7.9 (Fig. 2d). This event, along with the Banyak Islands SSE[35], SSEs in the Mexican subduction zone[36], Alaskan SSEs[37] and the pre-Tohoku SSE[3,33,34], represent some of the largest recorded SSEs. As a result of the low slip rates, such events can be difficult to detect in geodetic time series, since they may not be fast enough to cause a reversal in motion or show the obvious nonlinear patterns in the time series typically expected for SSEs. However, if we apply mechanical constraints on kinematic models we can test whether the observations are consistent with steady plate motion or are more compatible with a long-lived transient slip event. These methods can also be applied to estimate a more realistic seismic and tsunami hazard for subduction zones where near-trench model resolution is limited[31]. A similar method was used to detect slow, sustained creep migration along the Cascadia megathrust[38]. Such an approach has the potential to lower the threshold at which we can detect transient slip behaviour on a megathrust.

SSEs on velocity-strengthening faults

Comparing the region inferred to slip in the 1829–1861 SSE with coseismic and postseismic slip from the 2005 M_w 8.6 Nias earthquake (Fig. 2c), it appears that the 1829–1861 SSE occurred in a velocity-strengthening region[23]. Rate-and-state friction modelling of the postseismic slip for the 2005 earthquake suggests that the shallow megathrust is likely under low effective confining pressures and exhibits weakly velocity-strengthening behaviour[24].

We constructed a rate-and-state frictional model (Fig. 3) which shows that the observations of ~100 years of quiescence of shallow fault motion (1738–1829) can be explained by the response of a velocity-strengthening fault to a sudden fluid expulsion event

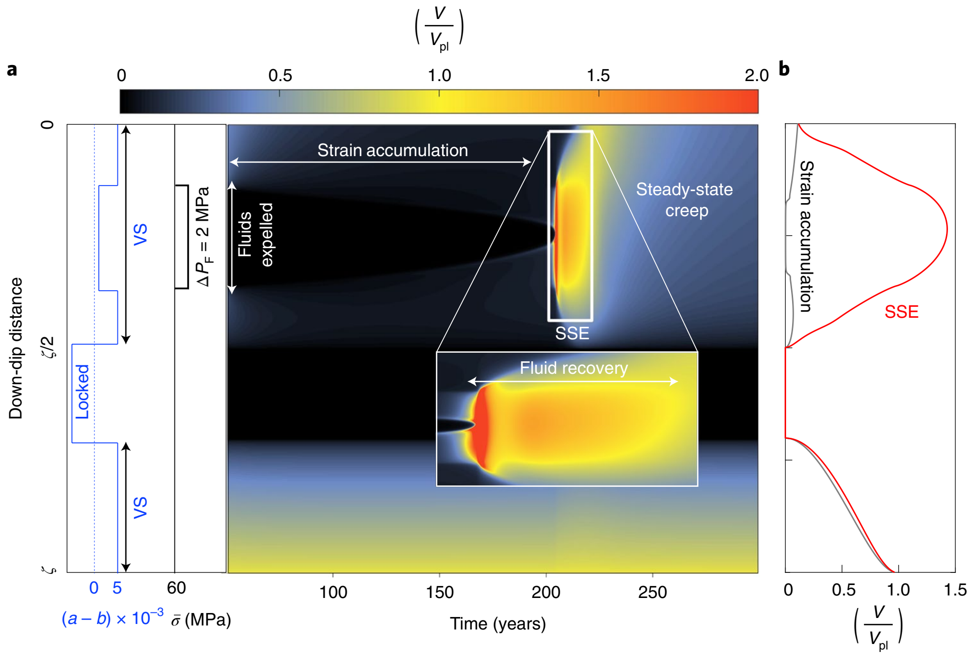

Fig. 3 | Numerical model of an SSE on a velocity-strengthening fault. a, Temporal evolution of normalized slip velocity (colours) leading up to and during a shallow SSE, and frictional parameters *a* – *b* (blue) and effective confining stress (black) used in the simulation (left). Fluid expulsion-driven clamping is prescribed at $t = 50$ years. This is followed by ~150-year-long strain accumulation. An SSE nucleates spontaneously and continues to slip for ~25 years, corresponding to the period over which fluid pressures are restored (inset). **b**, Representative normalized slip velocity profiles for the pre-SSE at $t = 150$ years (grey) and the SSE at $t = 210$ years (red).

early in the earthquake cycle (Fig. 3a and Extended Data Fig. 5). As faults can be regulatory agents for the transfer of fluids (fault-valve behaviour)[39,40], the release of fluids due to the breakage of permeability seals, possibly caused by the propagation of a past earthquake into this section of the megathrust[41–43] (at some time before 1738) or by strong shaking caused by passing earthquake waves[44], abruptly increases the confining pressures on the fault segment and causes it to become clamped (Fig. 3a). We model this as an instantaneous drop in pore-fluid pressure ($\Delta P_F = -2$ MPa) with a resulting normal stress increase. This is followed by a period of strain accumulation on the partially drained fault for up to centuries (Figs. 3b and 4). As the stresses and the stressing rates on the clamped fault increase over the following ~100 years, the fault is perturbed away from steady state (due to elastic interaction from the creep front migrating inwards) and nucleates a transient slip event with slip rates comparable to the plate velocity[40] (Fig. 3). Assuming normal stress recovery at a kinematically imposed linear rate as a proxy for slip rate modulated gouge compaction, which raises pore pressure[41,45,46] (see Methods and Supplementary Section S1), the fault which had just initiated accelerated creep is further destabilized as it returns to its undrained state (Fig. 4). The resulting SSE continues for decades with near-constant slip rates comparable to those observed between 1829–1861 at Simeulue (Fig. 4).

SSEs are typically modelled in the rate-and-state frictional framework as spontaneously nucleating instabilities on velocity-weakening faults[4–6,8]. The instability in these models is limited to an aseismic slip rate by a host of processes which ensure that, with increasing slip, the elastic energy release exceeds frictional strength loss[4–6,8]. Other models proposed to explain SSE, not dependent on velocity-weakening friction, are typically applicable at depths hot enough that the rheology of the rocks is brittle–ductile[15–17] and hence are not relevant for our observations. Alternate models of SSE in the brittle domain include nucleation on a fault with velocity-weakening friction at low velocities and a switch to velocity-strengthening friction at increased velocities[12,13]. While this model is plausible, such behaviour is not ubiquitous—it has mainly been seen in halite and certain types of serpentinite gouges[47]. The shallow velocity-strengthening section of the Sunda megathrust may have localized within layer silicates in the subducting sedimentary package[48]. The frictional properties of these rocks have not been tested at the slip rates relevant to this study; however, they have been noted to be purely velocity-strengthening over the ranges (0.1–10 μm s^{-1}) testable with experimental setups[47,49]. In this study, we provide a new mechanism to explain SSEs, by destabilizing a velocity-strengthening fault with normal stress variations likely related to pore-fluid migration from the subducting sedimentary package into fault gouge (Fig. 4). Recent theoretical work on this topic shows that the full incorporation of poroelastic effects into frictional behaviour on faults indeed leads to mildly unstable behaviour on velocity-strengthening faults, which may explain the mechanics of SSEs[50].

The results of our study force us to rethink our understanding of the nucleation and propagation of SSEs in a frictional framework. Given that the habitat of long-term SSEs at the down-dip edge of subduction zones is a region of high fluid pressure originating from dehydration reactions releasing fluids from sediments which are sealed by silica precipitation near the mantle wedge corner[9,11,41,51,52], it seems plausible that earthquake-cycle-driven drainage and restoration of pore fluids along the fault may control the occurrence of megathrust SSEs (Fig. 4) without any need to invoke complicated competing mechanisms to nucleate and then stabilize frictional instabilities on velocity-weakening faults.

A test for the applicability of this mechanism is to see whether regions hosting long-term SSEs overlap with afterslip following large earthquakes, since afterslip is a typical sign of velocity-strengthening behaviour. Sections of the megathrust in Nankai[53,54] as well as in Ecuador[55,56] appear to demonstrate this overlap of afterslip and SSE, thereby adding observational credence to our hypothesis. A different way to look for observations of this mechanism at play

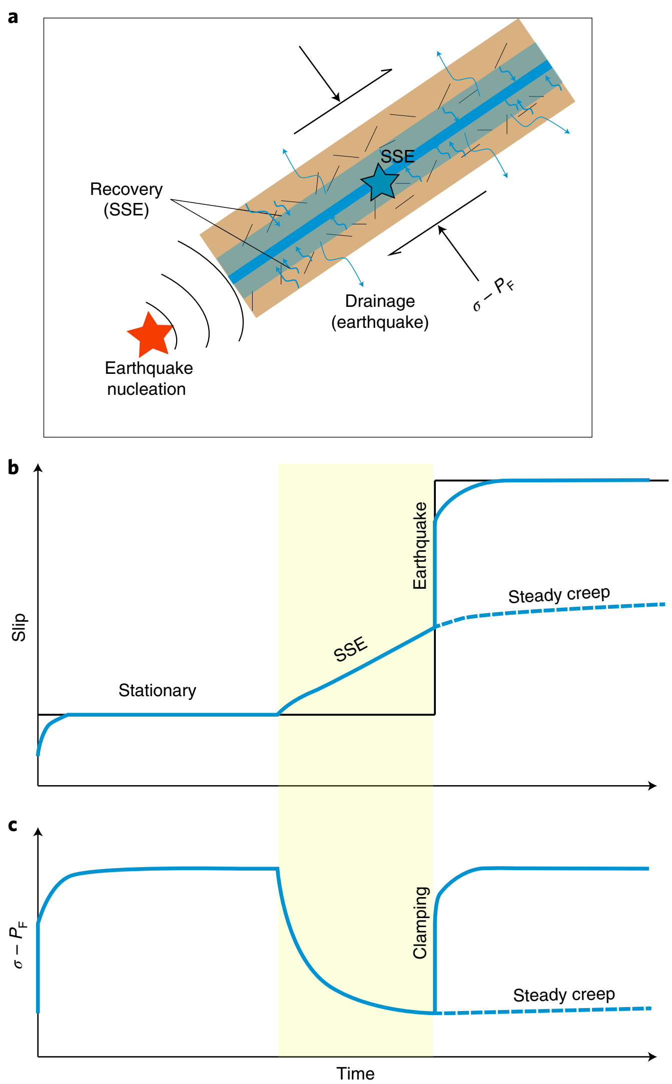

Fig. 4 | Illustration of the pore-fluid-driven SSE model presented in this paper. a–c, The fractured fault gouge governed by velocity-strengthening friction (**a**) is sealed and compacted by slow shear[41,45,46] during an SSE, leading to an increase in pore-fluid pressure (P_F) on the megathrust (decrease in effective normal stress; $\bar{\sigma} = \sigma - P_F$), as shown in the slip (**b**) and $\bar{\sigma}$ (**c**). Following the SSE period, two possibilities are shown: (1) an earthquake nucleates elsewhere and breaks permeability seals as it propagates into the shallow megathrust, draining the fault and increasing $\bar{\sigma}$ (thick line); (2) the SSE terminates, and the unlocked section of the fault resumes its steady-state creep, with negligible change in $\bar{\sigma}$ (dashed line).

in the modern instrumental record is to compare locations and timing records of seismicity within the forearc and/or the subducting oceanic crust with megathrust creep rates. Compared with the SSE period, we expect a cessation of plate boundary creep, due to expulsion of pore fluids, to preclude an increase in off-fault microseismicity (caused by released fluids travelling through the host rock). In other words, we expect an anti-correlation between off-fault seismicity and megathrust creep rates.

Implications for megathrust earthquakes

SSEs occurring on shallow megathrusts load neighbouring seismogenic sections of the fault, bring them closer to failure and pose a major earthquake and tsunami hazard[10]. There is precedent, in the case of the Sunda megathrust, for a close temporal relationship between multi-year SSEs and great plate boundary earthquakes. The 1829–1861 SSE discussed in this study was followed by a M_w ~8.5 earthquake[20], and the Andaman segment (further north) experienced a SSE from 2001–2004 along the shallow megathrust which was followed by the 2004 M_w 9.2 Sumatra–Andaman earthquake[57]. Creeping faults by themselves may not present a significant hazard, but their interactions with neighbouring segments make them unexpectedly dangerous[58].

Looking forward, a potential area of concern is the southernmost section of the Sunda megathrust, near Enggano Island. There, we interpret the global positioning system (GPS) data as indicative of a multi-year SSE along the shallow megathrust while the seismogenic domain is locked and accumulating strain (Fig. 5). This section of the megathrust was previously assumed not to accumulate any strain due to the observation of negligible trench-normal motion in the horizontal velocities derived from a continuous GPS site[59]. However, once we account for the vertical velocities, which show rapid subsidence (Fig. 5b), we find that such a signal is incompatible with steady aseismic creep on the megathrust. Instead, we show that frictional locking of the seismogenic zone of the megathrust in concert with a long-lived shallow SSE may be cancelling out landward motion while enhancing the subsidence of the island (Fig. 5c). With an improved understanding of the interplay between the locked seismogenic zones, shallow SSEs and the associated time series, we conclude that the hazard to the communities living near this section of the megathrust is potentially higher than was previously thought, and models of risk and mitigation strategies need updating.

Online content

Any methods, additional references, Nature Research reporting summaries, source data, extended data, supplementary information, acknowledgements, peer review information; details of author contributions and competing interests; and statements of data and code availability are available at https://doi.org/10.1038/s41561-021-00727-y.

Received: 24 March 2020; Accepted: 9 March 2021;
[redacted]

References

1. Michel, S., Gualandi, A. & Avouac, J. P. Similar scaling laws for earthquakes and Cascadia slow-slip events. *Nature* **574**, 522–526 (2019).
2. Gomberg, J., Wech, A., Creager, K., Obara, K. & Agnew, D. Reconsidering earthquake scaling. *Geophys. Res. Lett.* **43**, 6243–6251 (2016).
3. Bürgmann, R. The geophysics, geology and mechanics of slow fault slip. *Earth Planet. Sci. Lett.* **495**, 112–134 (2018).
4. Chen, T. & Lapusta, N. Scaling of small repeating earthquakes explained by interaction of seismic and aseismic slip in a rate and state fault model. *J. Geophys. Res. Solid Earth* **114**, B01311 (2009).
5. Liu, Y. & Rice, J. R. Aseismic slip transients emerge spontaneously in three-dimensional rate and state modeling of subduction earthquake sequences. *J. Geophys. Res. Solid Earth* **110**, B08307 (2005).
6. Liu, Y. & Rice, J. R. Spontaneous and triggered aseismic deformation transients in a subduction fault model. *J. Geophys. Res. Solid Earth* **112**, B09404 (2007).
7. Liu, Y. & Rice, J. R. Slow slip predictions based on granite and gabbro friction data compared to GPS measurements in northern Cascadia. *J. Geophys. Res. Solid Earth* **114**, B09407 (2009).
8. Segall, P., Rubin, A. M., Bradley, A. M. & Rice, J. R. Dilatant strengthening as a mechanism for slow slip events. *J. Geophys. Res. Solid Earth* **115**, B12305 (2010).
9. Audet, P. & Kim, Y. H. Teleseismic constraints on the geological environment of deep episodic slow earthquakes in subduction zone forearcs: a review. *Tectonophysics* **670**, 1–15 (2016).
10. Saffer, D. M. & Wallace, L. M. The frictional, hydrologic, metamorphic and thermal habitat of shallow slow earthquakes. *Nat. Geosci.* **8**, 594–600 (2015).
11. Audet, P. & Schaeffer, A. J. Fluid pressure and shear zone development over the locked to slow slip region in Cascadia. *Sci. Adv.* **4**, eaar2982 (2018).
12. Hawthorne, J. C. & Rubin, A. M. Laterally propagating slow slip events in a rate and state friction model with a velocity-weakening to velocity-strengthening transition. *J. Geophys. Res. Solid Earth* **118**, 3785–3808 (2013).

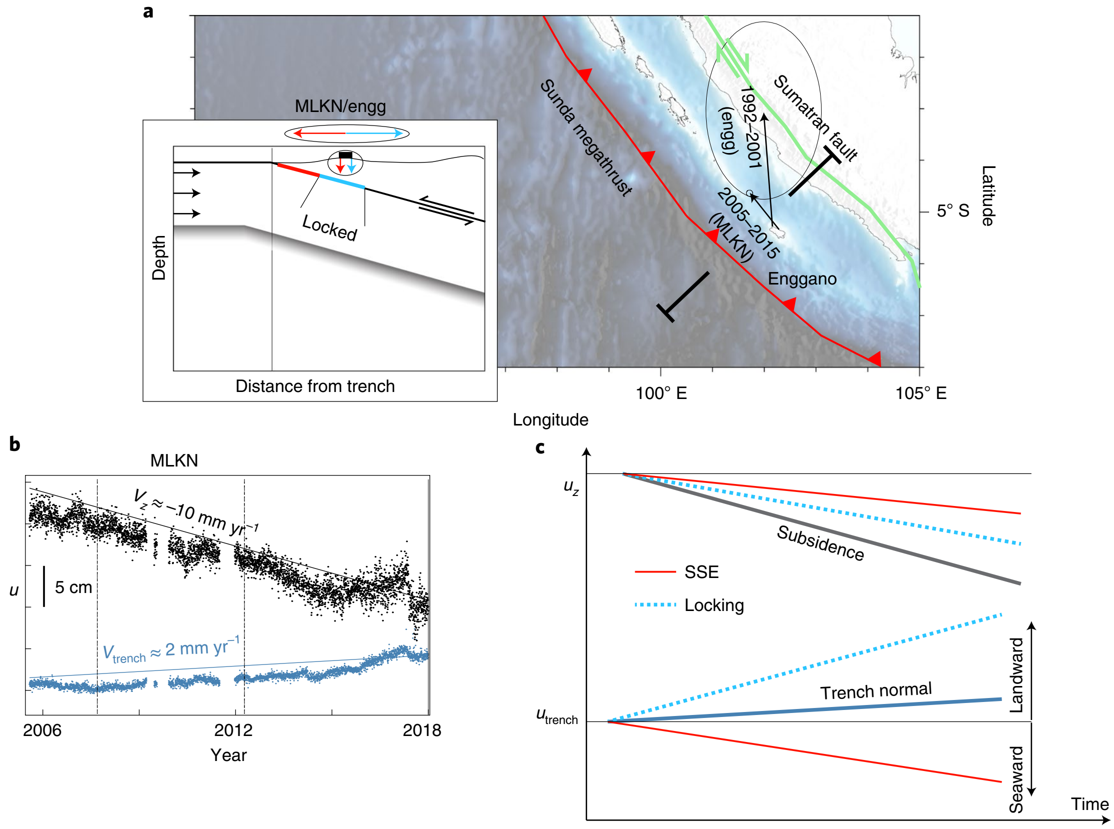

Fig. 5 | A possible ongoing long-lived SSE near Enggano Island. a, The horizontal velocities from a campaign site (engg, 1992–2001) and a continuous site (MLKN, 2005–2015) show a marked change in amplitude and direction, which we infer as the joint effect of frictional locking and an SSE. The inset shows a schematic cross-section of a locked seismogenic zone (cyan) and a shallow SSE (red) and their respective velocity predictions at Enggano. **b**, Displacement time series for MLKN with coseismic steps in 2007 and 2012 removed, showing trench-normal motion (blue) and vertical motion (black). **c**, Schematic showing how the surface displacement time series from the locked and SSE region interact to produce the observations at MLKN.

13. Im, K., Saffer, D., Marone, C. & Avouac, J.-P. Slip-rate-dependent friction as a universal mechanism for slow slip events. *Nat. Geosci.* **13**, 705–710 (2020).
14. Suzuki, T. & Yamashita, T. Dynamic modeling of slow earthquakes based on thermoporoelastic effects and inelastic generation of pores. *J. Geophys. Res. Solid Earth* **114**, B00A04 (2009).
15. Bernaudin, M. & Gueydan, F. Episodic tremor and slip explained by fluid-enhanced microfracturing and sealing. *Geophys. Res. Lett.* **45**, 3471–3480 (2018).
16. Lavier, L. L., Bennett, R. A. & Duddu, R. Creep events at the brittle ductile transition. *Geochem. Geophys. Geosyst.* **14**, 3334–3351 (2013).
17. Yin, A., Xie, Z. & Meng, L. A viscoplastic shear-zone model for deep (15–50 km) slow-slip events at plate convergent margins. *Earth Planet. Sci. Lett.* **491**, 81–94 (2018).
18. Marone, C. J., Scholtz, C. H. & Bilham, R. On the mechanics of earthquake afterslip. *J. Geophys. Res.* **96**, 8441–8452 (1991).
19. Scholz, C. H. Earthquakes and friction laws. *Nature* **391**, 37–42 (1998).
20. Meltzner, A. J. et al. Time-varying interseismic strain rates and similar seismic ruptures on the Nias–Simeulue patch of the Sunda megathrust. *Q. Sci. Rev.* **122**, 258–281 (2015).
21. Tsang, L. L. H. H., Meltzner, A. J., Hill, E. M., Freymueller, J. T. & Sieh, K. A paleogeodetic record of variable interseismic rates and megathrust coupling at Simeulue Island, Sumatra. *Geophys. Res. Lett.* **42**, 10585–10594 (2015).
22. Meltzner, A. J. et al. Persistent termini of 2004- and 2005-like ruptures of the Sunda megathrust. *J. Geophys. Res. Solid Earth* **117**, B04405 (2012).
23. Qiu, Q., Feng, L., Hermawan, I. & Hill, E. M. Coseismic and postseismic slip of the 2005 M_w 8.6 Nias–Simeulue earthquake: spatial overlap and localized viscoelastic flow. *J. Geophys. Res. Solid Earth* **124**, 2018JB017263 (2019).
24. Hsu, Y.-J. et al. Frictional afterslip following the 2005 Nias–Simeulue earthquake, Sumatra. *Science (80-.)* **312**, 1921–1926 (2006).
25. Melnick, D. et al. The super-interseismic phase of the megathrust earthquake cycle in Chile. *Geophys. Res. Lett.* **44**, 784–791 (2017).
26. Loveless, J. P. Super-interseismic periods: redefining earthquake recurrence. *Geophys. Res. Lett.* **44**, 1329–1332 (2017).
27. Simoes, M., Avouac, J. P., Cattin, R. & Henry, P. The Sumatra subduction zone: a case for a locked fault zone extending into the mantle. *J. Geophys. Res. Solid Earth* **109**, B10402 (2004).
28. Klingelhoefer, F. et al. Limits of the seismogenic zone in the epicentral region of the 26 December 2004 great Sumatra–Andaman earthquake: results from seismic refraction and wide-angle reflection surveys and thermal modeling. *J. Geophys. Res. Solid Earth* **115**, B01304 (2010).
29. Hippchen, S. & Hyndman, R. D. Thermal and structural models of the Sumatra subduction zone: implications for the megathrust seismogenic zone. *J. Geophys. Res. Solid Earth* **113**, B12103 (2008).
30. Almeida, R. et al. Can the updip limit of frictional locking on megathrusts be detected geodetically? Quantifying the effect of stress shadows on near-trench coupling. *Geophys. Res. Lett.* **45**, 4754–4763 (2018).
31. Lindsey, E. O. et al. Slip rate deficit and earthquake potential on shallow megathrusts. *Nat. Geosci.* https://doi.org/10.1038/s41561-021-00736-x (2021).
32. Mavrommatis, A. P., Segall, P. & Johnson, K. M. A physical model for interseismic erosion of locked fault asperities. *J. Geophys. Res. Solid Earth* **122**, 8326–8346 (2017).
33. Mavrommatis, A. P., Segall, P. & Johnson, K. M. A decadal-scale deformation transient prior to the 2011 M_w 9.0 Tohoku-oki earthquake. *Geophys. Res. Lett.* **41**, 4486–4494 (2014).
34. Mavrommatis, A. P., Segall, P., Uchida, N. & Johnson, K. M. Long-term acceleration of aseismic slip preceding the M_w 9 Tohoku-oki earthquake: constraints from repeating earthquakes. *Geophys. Res. Lett.* **42**, 9717–9725 (2015).
35. Tsang, L. L. H. et al. A 15 year slow-slip event on the Sunda megathrust offshore Sumatra. *Geophys. Res. Lett.* **42**, 6630–6638 (2015).
36. Radiguet, M. et al. Slow slip events and strain accumulation in the Guerrero gap, Mexico. *J. Geophys. Res. Solid Earth* **117**, B04305 (2012).
37. Li, S., Freymueller, J. & McCaffrey, R. Slow slip events and time-dependent variations in locking beneath Lower Cook Inlet of the Alaska–Aleutian subduction zone. *J. Geophys. Res. Solid Earth* **121**, 1060–1079 (2016).

38. Bruhat, L. & Segall, P. Coupling on the northern Cascadia subduction zone from geodetic measurements and physics-based models. *J. Geophys. Res. Solid Earth* **121**, 8297–8314 (2016).
39. Sibson, R. H. Implications of fault-valve behaviour for rupture nucleation and recurrence. *Tectonophysics* **211**, 283–293 (1992).
40. Perfettini, H. & Ampuero, J.-P. P. Dynamics of a velocity strengthening fault region: implications for slow earthquakes and postseismic slip. *J. Geophys. Res.* **113**, B09411 (2008).
41. Sibson, R. H. Stress switching in subduction forearcs: implications for overpressure containment and strength cycling on megathrusts. *Tectonophysics* **600**, 142–152 (2013).
42. Husen, S. & Kissling, E. Postseismic fluid flow after the large subduction earthquake of Antofagasta, Chile. *Geology* **29**, 847–850 (2002).
43. Hughes, K. L. H., Masterlark, T. & Mooney, W. D. Poroelastic stress-triggering of the 2005 M8.7 Nias earthquake by the 2004 M9.2 Sumatra–Andaman earthquake. *Earth Planet. Sci. Lett.* **293**, 289–299 (2010).
44. Materna, K., Bartlow, N., Wech, A., Williams, C. & Bürgmann, R. Dynamically triggered changes of plate interface coupling in southern Cascadia. *Geophys. Res. Lett.* **46**, 12890–12899 (2019).
45. Sibson, R. H. Conditions for fault-valve behaviour. *Geol. Soc. London Spec. Publ.* **54**, 15–28 (1990).
46. Sleep, N. H. & Blanpied, M. L. Creep, compaction and the weak rheology of major faults. *Nature* **359**, 687–692 (1992).
47. Moore, D. E. et al. in *The Seismogenic Zone of Subduction Thrust Faults* 317–345 (Columbia Univ. Press, 2007); https://doi.org/10.7312/dixo13866-011
48. Bradley, K. et al. Stratigraphic control of frontal décollement level and structural vergence and implications for tsunamigenic earthquake hazard in Sumatra, Indonesia. *Geochem. Geophys. Geosyst.* **20**, 1646–1664 (2019).
49. Saffer, D. M. & Marone, C. Comparison of smectite- and illite-rich gouge frictional properties: application to the updip limit of the seismogenic zone along subduction megathrusts. *Earth Planet. Sci. Lett.* **215**, 219–235 (2003).
50. Heimisson, E. R., Dunham, E. M. & Almquist, M. Poroelastic effects destabilize mildly rate-strengthening friction to generate stable slow slip pulses. *J. Mech. Phys. Solids* **130**, 262–279 (2019).
51. Hyndman, R. D. & Peacock, S. M. Serpentinization of the forearc mantle. *Earth Planet. Sci. Lett.* **212**, 417–432 (2003).
52. Audet, P., Bostock, M. G., Christensen, N. I. & Peacock, S. M. Seismic evidence for overpressured subducted oceanic crust and megathrust fault sealing. *Nature* **457**, 76–78 (2009).
53. Johnson, K. M. & Tebo, D. Capturing 50 years of postseismic mantle flow at Nankai Subduction Zone. *J. Geophys. Res. Solid Earth* **123**, 10091–10106 (2018).
54. Yarai, H. & Ozawa, S. Quasi-periodic slow slip events in the afterslip area of the 1996 Hyuga-nada earthquakes, Japan. *J. Geophys. Res. Solid Earth* **118**, 2512–2527 (2013).
55. Rolandone, F. et al. Areas prone to slow slip events impede earthquake rupture propagation and promote afterslip. *Sci. Adv.* **4**, 2–10 (2018).
56. Tsang, L. L. H. et al. Imaging rapid early afterslip of the 2016 Pedernales earthquake, Ecuador. *Earth Planet. Sci. Lett.* **524**, 115724 (2019).
57. Paul, J. & Rajendran, C. P. Short-term pre-2004 seismic subsidence near South Andaman: is this a precursor slow slip prior to a megathrust earthquake? *Phys. Earth Planet. Inter.* **248**, 30–34 (2015).
58. Harris, R. A. Large earthquakes and creeping faults. *Rev. Geophys.* **55**, 169–198 (2017); https://doi.org/10.1002/2016RG000539
59. Prawirodirdjo, L., McCaffrey, R., Chadwell, C. D., Bock, Y. & Subarya, C. Geodetic observations of an earthquake cycle at the Sumatra subduction zone: role of interseismic strain segmentation. *J. Geophys. Res.* **115**, B03414 (2010).

Publisher's note Springer Nature remains neutral with regard to jurisdictional claims in published maps and institutional affiliations.

Methods

Coral time series analysis. The coral time series for sites LBJ, UTG, SLR and SMB are taken from published data[20]. The measurement uncertainty at each point used in the velocity extraction is 2 cm. This uncertainty estimate comes from an observation that the largest measurement bias between two corals from the same site was 8 cm (ref. [20]). We interpret that as the 99% confidence level extremum (3σ).

It is obvious that a simple linear least-squares fit cannot explain the time series, and so we explore three different hypotheses: (1) a quadratic least-squares fit, invoking a continuous acceleration, (2) piece-wise linear fits with the timing of the change in velocities (T_{change}) being common to all the sites and (3) piece-wise linear fits treating each site independently.

We then assess the error improvement using the F test. For the piece-wise linear fits, we add an equality constraint such that the fitted function is continuous across T_{change}. We estimate the mean and covariance of the fitted parameters using simple matrix inversion since the addition of equality constraints to the linear inverse problem can be thought of as a typical least-squares problem with additional Lagrangian multipliers, which means the posterior distribution is still Gaussian. For a given dataset $\mathbf{d}$, design matrix G (a function of T_{change}) and weighting function W, we estimate the distribution of the model parameters $\mathbf{m} \sim N(\hat{\mathbf{m}}, C_{\mathbf{m}})$ subject to an equality constraint $A\mathbf{m}=\mathbf{b}$ as

$$\hat{\mathbf{m}} = \left(G^{\mathrm{T}}WG\right)^{-1} \left[G^{\mathrm{T}}\mathbf{d} - A^{\mathrm{T}}\left(A\left(G^{\mathrm{T}}WG\right)^{-1}A^{\mathrm{T}}\right)^{-1}\left(A\left(G^{\mathrm{T}}WG\right)^{-1}G^{\mathrm{T}}\mathbf{d}-\mathbf{b}\right)\right] \tag{1}$$

$$C_{\mathbf{m}} = \sigma^2 \left(\left(G^{\mathrm{T}}WG\right)^{-1} - \left(G^{\mathrm{T}}WG\right)^{-1}A^{\mathrm{T}}\left(A\left(G^{\mathrm{T}}WG\right)^{-1}A^{\mathrm{T}}\right)^{-1}A\left(G^{\mathrm{T}}WG\right)^{-1}\right) \tag{2}$$

The uncertainties in m associated with T_{change} are non-Gaussian but are an order of magnitude lower than $C_{\mathbf{m}}$, which is why we report only $C_{\mathbf{m}}$. σ^2 is the least-squares misfit when we use $\hat{\mathbf{m}}$ to fit the data.

The reduced χ^2 from the different hypotheses is shown in Extended Data Fig. 1b. From the F test, we conclude that piece-wise linear fits for a common $T_{\text{change}} = 1829$ across all sites is the most likely hypothesis. We do not use site SLR in subsequent analysis since the uncertainties in the velocities for the site are too large for the velocities to be meaningful.

SSE on a velocity-strengthening fault with normal stress perturbations. We can describe the variation of the friction coefficient μ as a function of velocity, v, and a state parameter, θ, using rate-and-state-dependent friction[60,61].

$$\mu = \mu_0 + a\log\frac{v}{v_0} + b\log\frac{v_0\theta}{L} \tag{3}$$

μ_0, v_0 are reference values of the friction coefficient and velocity, respectively, while L is the critical slip distance over which a population of frictional contacts evolve. We use the ageing law to describe state evolution[61]

$$\frac{\mathrm{d}\theta}{\mathrm{d}t} = 1 - \frac{v\theta}{L} \tag{4}$$

For a 2D plane-strain setup, at any given time t, consider the force balance on any fault segment of length $\mathrm{d}\zeta$, in the domain Ω, at a location ζ in the down-dip direction. There are two directions along which we resolve the forces acting on the system: (1) in the plane of shear, $\hat{\mathbf{d}}$, and (2) in the direction of the normal vector to the fault surface, $\hat{\mathbf{n}}$. Consider the force balance in the fault slip direction:

$$\dot{\tau}^{\infty}t + \int_{\Omega} K_{\tau}(\zeta,\Omega)\delta(\zeta,t)\,\mathrm{d}\zeta = \mu\left(v,\theta\right)\bar{\sigma} + \frac{G}{2v_{\mathrm{s}}}v \tag{5}$$

Here $\dot{\tau}^{\infty}$ is the far-field loading rate on the fault from the subducting plate model[62] with the trench-normal convergence rate, 40 mm yr^{-1}, taken from a regional plate motion model[63]. The integral over the fault domain Ω defines the elastic interaction kernel from the Green's function tensor K_{τ} and slip on the fault δ. The right-hand side contains the frictional stress (with uniform $\bar{\sigma} = 60$ MPa) and the radiation damping approximation (where G and v_{s} are the shear modulus and shear wave speed of the elastic medium, respectively) at seismic slip rates[64].

In the boundary element formulation, we can approximate the elastic interaction integral by a simple matrix multiplication for finite dislocations[65]. The time derivative of Eq. 5 gives us the momentum balance in two directions:

$$\begin{aligned} &(\hat{\mathbf{d}})\ \ \dot{\tau}^{\infty} + K_{\tau}v\left(\zeta,t\right) = \dot{\mu}\,\bar{\sigma} + \mu\,\dot{\bar{\sigma}} + \tfrac{G}{2v_{\mathrm{s}}}\,\dot{v} \\ &(\hat{\mathbf{n}})\ \ \dot{\bar{\sigma}} \rightarrow \ \text{kinematically imposed} \end{aligned} \tag{6}$$

We use the far-field stressing rate in the dip direction, and kinematically impose the stressing rates in the $\hat{\mathbf{n}}$ direction to model pore-fluid migration. The overdots indicate time derivatives of the appropriate quantities.

We can numerically integrate the coupled ordinary differential equations in Eq. 6 using a Runge–Kutta fourth-order method, subject to an initial condition. The initial value is provided by means of a velocity step derived from Eq. 5 for a sudden change in $\bar{\sigma}$ from t^- to t^+.

$$\begin{aligned} v^+ &= \left(v^-\right)^{\frac{\bar{\sigma}^-}{\bar{\sigma}^+}}\left(v_0\right)^{1-\frac{\bar{\sigma}^-}{\bar{\sigma}^+}}\exp\left(\frac{\left(\mu_0 + b\log\frac{v_0\vartheta^-}{L}\right)\left(\bar{\sigma}^- - \bar{\sigma}^+\right)}{a\bar{\sigma}^+}\right) \\ \theta^+ &= \theta^- \end{aligned} \tag{7}$$

We choose a value of $\bar{\sigma}^- - \bar{\sigma}^+ = -2$ MPa motivated by the magnitude of the stress drop necessary to generate a detectable transient[40] as well as by past studies that have proposed the MPa-scale rapid changes (drop) in pore pressure that are expected during or soon after great earthquakes[43].

We assume that $\dot{\bar{\sigma}}$ is 0 during the strain accumulation phase and is a linearly decreasing function of time once the SSE spontaneously nucleates (t_{SSE}), such that the integrated normal stress change over the SSE duration ΔT_{SSE} equals the initial normal stress perturbation $\left(\bar{\sigma}^- - \bar{\sigma}^+\right) = \Delta P_{\mathrm{F}}$ (Fig. 3a). We add the linear taper on $\dot{\bar{\sigma}}$ to create a simple model of slip-rate-dependent gouge compaction which causes pore-fluid pressures to rise, thereby lowering the effective confining stress ($\bar{\sigma}$) to its initial value before being perturbed ($\bar{\sigma}^-$) (refs. [41,46]).

$$\begin{aligned} \dot{\bar{\sigma}} &= 0 \qquad \left(t \in \left[t^+, t_{\text{SSE}}\right]\right) \\ \dot{\bar{\sigma}} &= \tfrac{2\Delta P_{\mathrm{F}}}{\Delta T_{\text{SSE}}}\left(1 - \tfrac{t - t_{\text{SSE}}}{\Delta T_{\text{SSE}}}\right) \qquad \left(t \in \left[t_{\text{SSE}}, t_{\text{SSE}} + \Delta T_{\text{SSE}}\right]\right) \end{aligned} \tag{8}$$

Inverse method to estimate SSE slip rates. We use physical constraints from Eq. 6 to develop our inverse method as follows. In the steady interseismic period, locked parts of the fault accumulate strain while creeping parts of the fault slip at time-invariant slip rates determined by the net shear stress rate at that location (Eq. 6), with $\dot{\mu} = \dot{\bar{\sigma}} = 0$. We can write this as

$$\begin{aligned} &\dot{\tau}^{\infty} + K_{\tau}v(\zeta,t) = 0 \quad \text{steady creep at available } \dot{\tau} \\ &\dot{\tau}^{\infty} + K_{\tau}v(\zeta,t) > 0 \quad \text{locked} \end{aligned} \tag{9}$$

We segment the fault into four regions, using three free parameters ζ_{up}, ζ_{down}, ζ_{free} (Extended Data Fig. 2a). Region 1 is a creeping zone which extends from the free surface to ζ_{up}. Region 2 is a locked zone between ζ_{up} and ζ_{down}. Region 3 is a creeping zone between ζ_{down} and ζ_{free}. Region 4 creeps at the plate rate below ζ_{free}.

The data for the inverse problem are the vertical velocities we computed using Eqs. 1 and 2. Since we use a plane-strain approximation and the stations do not exactly fall on a 2D transect, we calculate weighted average velocities and uncertainties from the three sites to represent the vertical motion of Simeulue Island in a representative cross-section (Fig. 2).

The slip rate to surface velocity relations are taken from analytical solutions for edge dislocations in plane strain for elastic media[65,66] and a geometric setup applicable to the Sunda megathrust[62,63,67]. The misfit between the data and model-predicted velocities is assumed to follow an unbiased multivariate Gaussian distribution with unknown variance. We sample the posterior distribution of the free parameters using a Markov chain Monte Carlo method (slice sampling)[68,69]. We use this method to estimate the steady-state slip rates on the Sunda megathrust for 1738–1829 as well as 1829–1861 (Fig. 2 and Extended Data Fig. 3).

For the case where we assume that a transient slip event occurs as a quasi-steady process, we parameterize a continuously connected section of fault to have a constant slip rate (within its domain, as well as over the time period 1829–1861). This velocity is superimposed on the jointly estimated 1738–1829 slip rate distribution from the steady-state inversion. We use slice sampling to sample the up-dip and down-dip extent of the transient as well as its slip rate $\left(\zeta_{\text{up}}^{\text{trans}}, \zeta_{\text{down}}^{\text{trans}}, V_{\text{trans}}\right)$ in addition to the steady-state locking/creeping parameters $\left(\zeta_{\text{up}}^{\text{lock}}, \zeta_{\text{down}}^{\text{lock}}, \zeta_{\text{free}}^{\text{lock}}\right)$ for the 1738–1829 period (Extended Data Fig. 4).

Data availability

The coral data used in this paper are from ref. [20] (https://doi.org/10.1016/j.quascirev.2015.06.003), also available at https://doi.org/10.21979/N9/5QCLZX. The daily RINEX files for the GNSS station MLKN are available for public download at ftp://ftp.earthobservatory.sg/SugarData. The processed time series is provided at https://doi.org/10.21979/N9/LMK36Z. Topography and bathymetry plotted in Figs. 1 and 5 are from the ETOPO1 dataset available at https://doi.org/10.7289/V5C8276M. The figures in this paper were made using MATLAB and Generic Mapping Tools[70].

Code availability

All computations in this study were carried out using MATLAB; code is available at https://researchdata.ntu.edu.sg/dataverse/longlivedsse/.

References

60. Dieterich, J. H. Modeling of rock friction experimental 1. Results and constitutive equations. *J. Geophys. Res.* **84**, 2161–2168 (1979).
61. Ruina, A. Slip instability and state variable friction laws. *J. Geophys. Res. Solid Earth* **88**, 10359–10370 (1983).
62. Kanda, R. V. S. & Simons, M. An elastic plate model for interseismic deformation in subduction zones. *J. Geophys. Res. Solid Earth* **115**, B03405 (2010).
63. Bradley, K. E., Feng, L., Hill, E. M., Natawidjaja, D. H. & Sieh, K. Implications of the diffuse deformation of the Indian Ocean lithosphere for slip partitioning of oblique plate convergence in Sumatra. *J. Geophys. Res. Solid Earth* **122**, 572–591 (2017).
64. Rice, J. R. Spatio-temporal complexity of slip on a fault. *J. Geophys. Res.* **98**, 9885 (1993).
65. Segall, P. *Earthquake and Volcano Deformation. Van Nostrand's Scientific Encyclopedia* (Princeton Univ. Press, 2010); https://doi.org/10.1515/9781400833856
66. Okada, Y. Internal deformation due to shear and tensile faults in a half space. *Bull. Seismol. Soc. Am.* **82**, 1018–1040 (1992).
67. Hayes, G. P. et al. Slab2, a comprehensive subduction zone geometry model. *Science (80-.)* **362**, 58–61 (2018).
68. Neal, R. M. Slice sampling. *Ann. Stat.* **31**, 705–767 (2003).
69. Lindsey, E. O. & Fialko, Y. Geodetic slip rates in the southern San Andreas Fault system: effects of elastic heterogeneity and fault geometry. *J. Geophys. Res. Solid Earth* **118**, 689–697 (2013).
70. Wessel, P. & Smith, W. H. F. New, improved version of generic mapping tools released. *Eos* **79**, 579–579 (1998).

Acknowledgements

This research was supported by the National Research Foundation Singapore under a Singapore NRF Investigatorship to E.M.H. (proposal ID NRF-NRFI05–2019–0009), Singapore NRF Fellowship to A.J.M. (NRF-NRFF11–2019–0008), the Earth Observatory of Singapore (EOS), the National Research Foundation of Singapore, and the Singapore Ministry of Education under the Research Centers of Excellence initiative. Data for the Enggano GPS station MLKN were taken from the SuGAr network maintained by EOS and the Indonesian Institute of Sciences (LIPI). This is EOS contribution number 335.

Author contributions

R.M., A.J.M., L.L.H.T. and E.M.H. designed the study. R.M. and E.O.L. developed the inverse method. R.M. conducted the data analysis and developed the numerical models for the study. L.F. processed the GPS data and provided the time series for MLKN. All authors jointly wrote the paper.

Competing interests

The authors declare no competing interests.

Additional information

Extended data is available for this paper at https://doi.org/10.1038/s41561-021-00727-y.

Supplementary information The online version contains supplementary material available at https://doi.org/10.1038/s41561-021-00727-y.

Correspondence and requests for materials should be addressed to R.M.

Peer review information *Nature Geoscience* thanks Daniel Melnick and the other, anonymous, reviewer(s) for their contribution to the peer review of this work. Primary Handling Editor: Stefan Lachowycz.

Reprints and permissions information is available at www.nature.com/reprints.

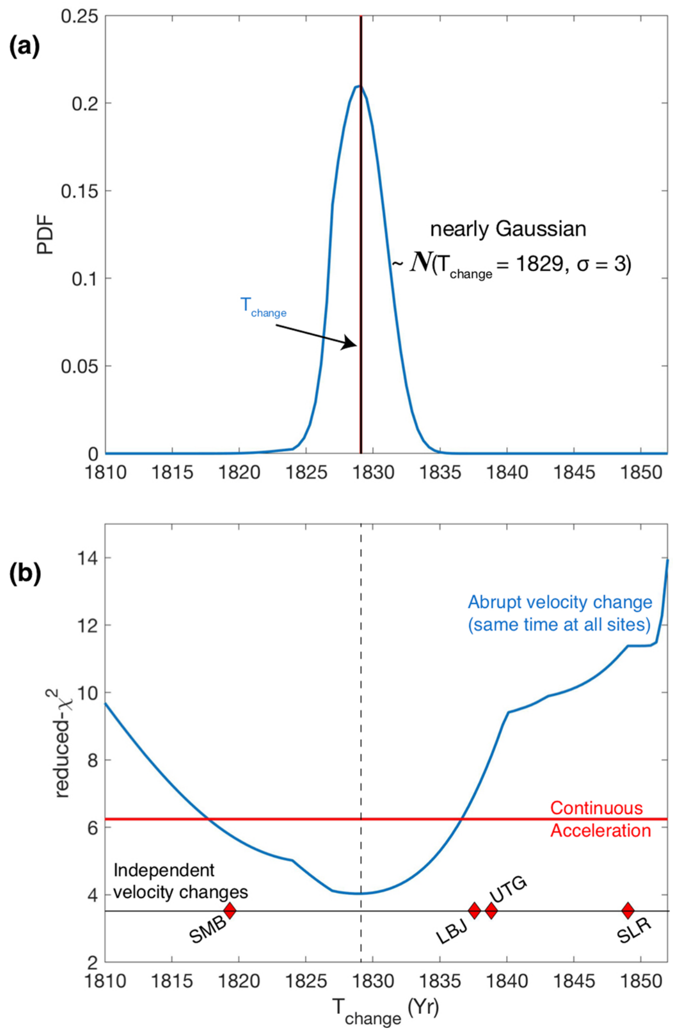

Extended Data Fig. 1 | Testing multiple hypotheses to explain the trends in the coral time series. Testing multiple hypotheses to explain the trends in the coral time series. **a**, Assuming a piecewise linear fit for the time series with a common timing for the velocity change, T_{change}, we evaluate the misfit (with Gaussian error statistics - thick blue line). **b**, We evaluate the reduced χ^2 and the significance of error reduction using the F-test for the following hypotheses: piecewise linear fits with an abrupt velocity change at T_{change} (blue line - this is the preferred model), continuous acceleration (red line) and piecewise linear fits with an abrupt velocity change whose timing varies for each station (red diamonds).

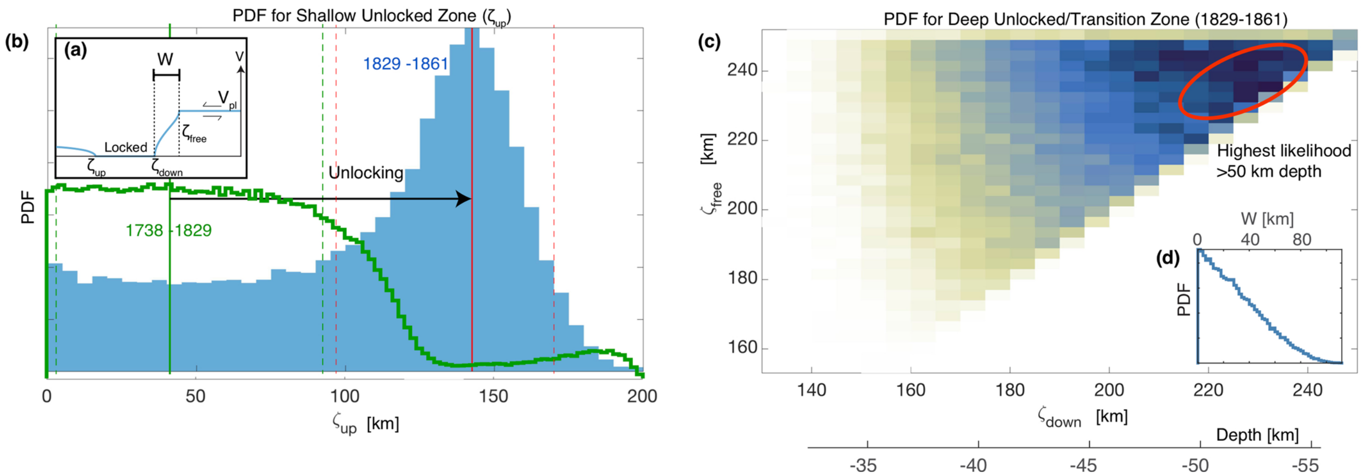

Extended Data Fig. 2 | PDFs for spatial extent of locked and creeping regions on the megathrust. PDFs for spatial extent of locked and creeping regions on the megathrust. **a**, Geometric setup and terminology used to describe the 4 segments of the megathrust: shallow creeping, frictionally locked, unlocked/transition zone and freely sliding plate boundary. **b**, PDFs of the spatial extent of ζ_{up} for two time periods (1738–1829 and 1829–1861) assuming steady frictional locking and creep governs the evolution of slip on the megathrust. Maximum aposteriori probability (MAP) of ζ_{up} for 1738–1829 is shown as green thick line (95 % confidence interval - thin green lines); MAP of ζ_{up} for 1829–1861 is shown as red thick line (95 % confidence interval - thin red lines). To explain the 1829–1861 coral observations with only steady interseismic processes, the upper limit of the locked zone ζ_{up} would have to migrate down-dip by 50–100 km while the (**c**) deeper transition zone ζ_{down} would have to migrate to a depth of 50–60 km. **d**, The transition from ζ_{down} to ζ_{free} (W) would have to narrow to infinitesimal widths (pdf is maximum at W=0) making this model unphysical.

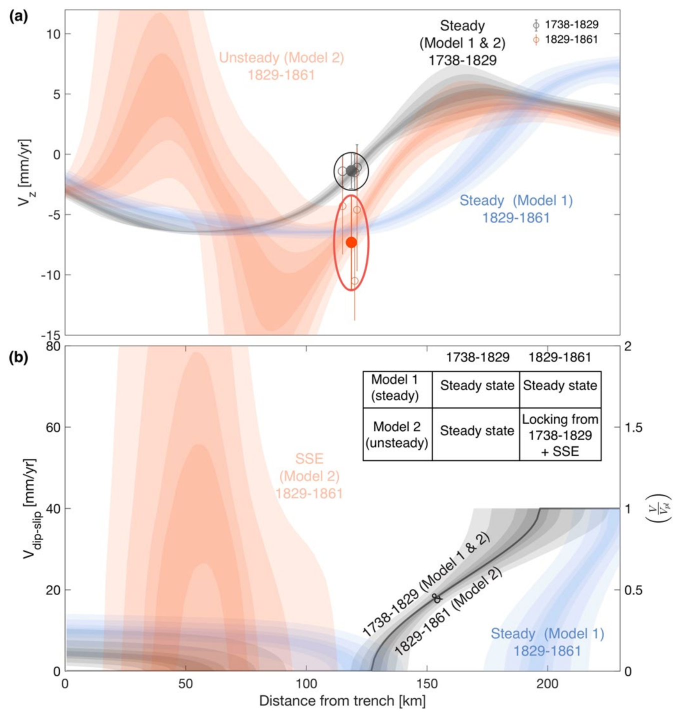

Extended Data Fig. 3 | Observations and modelling results for the 18th-19th century coral record in Simeulue. Observations and modelling results for the 18th-19th century coral record in Simeulue. **a**, Subsidence rates for the two time periods, 1738–1829 (grey) and 1829-1861 (red). We assume the velocities from each epoch collectively show the average response of southern Simeulue Island to tectonic changes (filled error bar). The individual site vertical velocities are plotted with error bars, while the model predictions are shown as polygons (67% confidence level, with darker colours showing regions closer to the median). **b**, Estimated slip rate for 1738-1829 is shown as a grey polygon (67% confidence level). The slip rate for the period 1829-1861 is estimated using two different models: (1) steady interseismic processes with a change in locked/unlocked regions (blue polygon), (2) SSE (orange polygon) superimposed on the existing locking from 1738-1829.

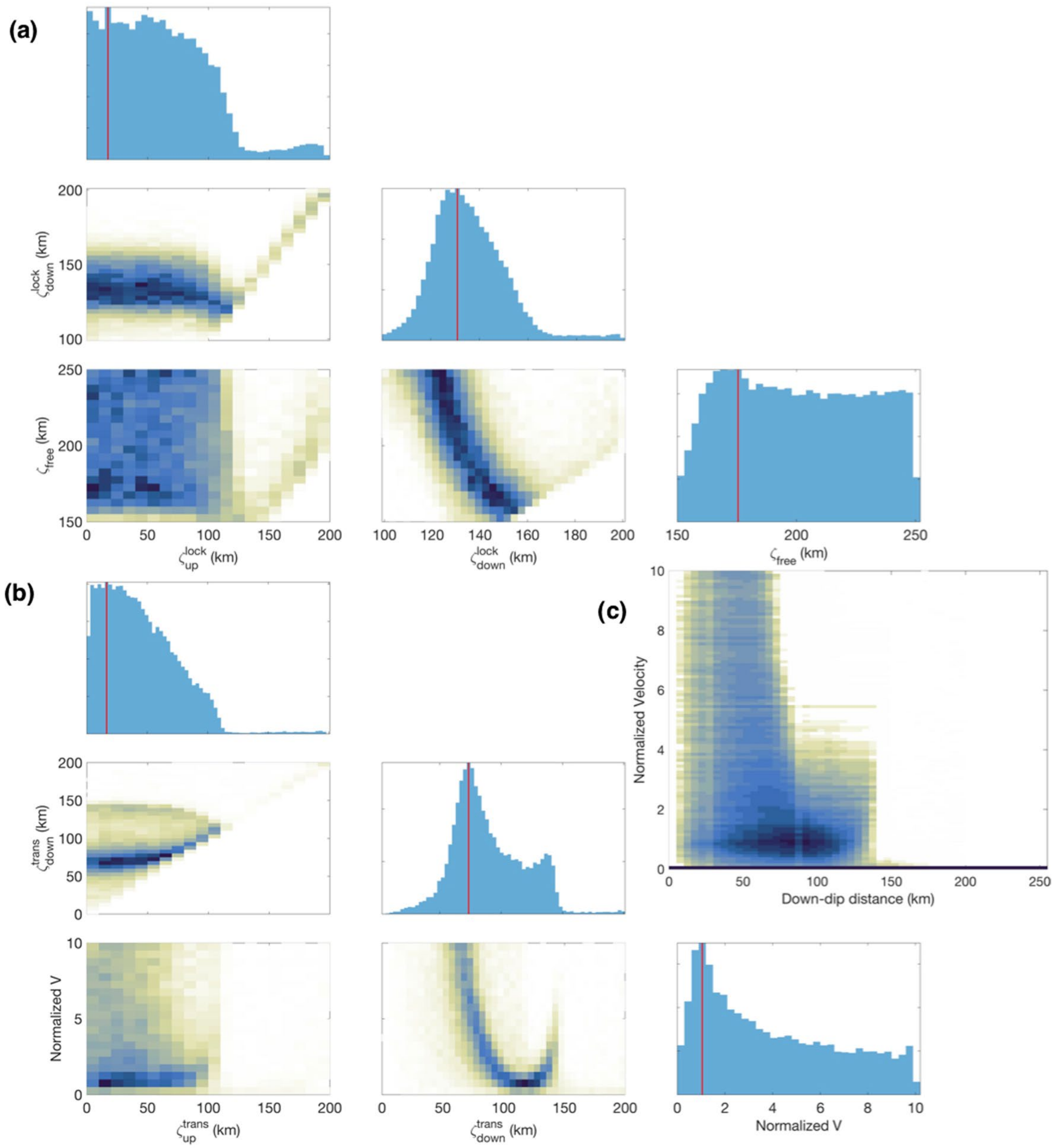

Extended Data Fig. 4 | 1-d and 2-d marginal PDFs of the spatial parameters. 1-d and 2-d marginal PDFs of the spatial parameters (ζ_{up-dip}, $\zeta_{down-dip}$, ζ_{free} in Extended Data Fig. 2a) describing (**a**) frictional domains for a model where we assume the 1738-1829 velocity field is attributed to steady frictional behaviour on the Sunda megathrust followed by (**b**) the occurrence of a long-lived transient slip event (SSE) from 1829-1861. The SSE is estimated to occur between ζ_{up} and ζ_{bot} with an average slip rate of V_{trans} (mm/yr) (we normalize this by the plate rate V_{pl}). (See Methods for a more detailed description of all parameters). **c**, We show the joint distribution of SSE slip rate and the along-dip location where this slip occurred. The darker colours show a higher value of the PDF; the red line in the 1-d marginal PDFs is the maximum aposteriori estimate.

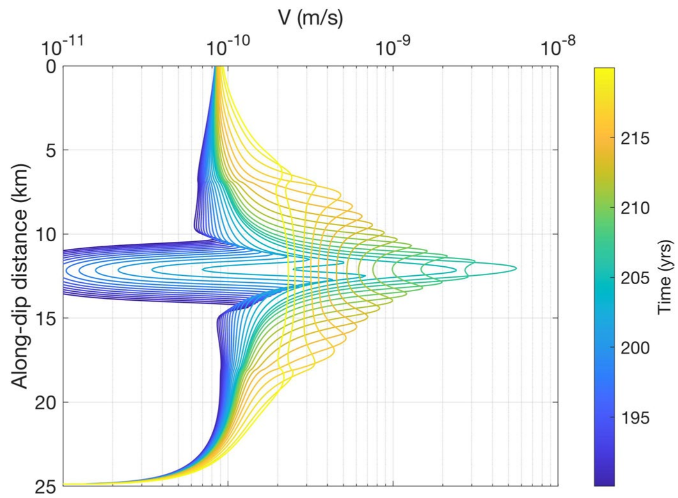

Extended Data Fig. 5 | Snapshots through time of a frictional instability on a velocity strengthening fault. Snapshots through time of a frictional instability on a velocity strengthening fault. A steady-state creeping fault was perturbed early in the simulation (t = 50 yrs) by a pore-fluid expulsion event and allowed to evolve. In this simulation we do not allow additional weakening from pore-pressure recovery on the fault. The colors represent different time periods (t = 190 to 230 yrs) - from the initial acceleration of the SSE (blue) until the instability is arrested and the fault resumes creeping at its steady rate velocity (yellow). The SSE nucleates at the 12–14 km position on the simulated fault, as the fault is trying to recover to its steady state creep rate. However, an overshoot of slip rates occurs leading to a pulse of high slip rate at the center of the simulated fault. The transition from creep at below 10^{-10} m/s to the accelerated slip pulse of ~ 10^{-8} m/s occurs in a short period of time (1-2 yrs). This instability is then damped out and is smeared over the available fault area over 10–15 years.